



CHORUS

This is the accepted manuscript made available via CHORUS. The article has been published as:

Configuration-specific electronic structure of strongly interacting interfaces: TiOPc on Cu(110)

Bret Maughan, Percy Zahl, Peter Sutter, and Oliver L. A. Monti

Phys. Rev. B **96**, 235133 — Published 21 December 2017

DOI: [10.1103/PhysRevB.96.235133](https://doi.org/10.1103/PhysRevB.96.235133)

Configuration-Specific Electronic Structure of Strongly Interacting Interfaces: TiOPc on Cu(110)

Bret Maughan,¹ Percy Zahl,² Peter Sutter^{2,3} and Oliver L. A. Monti^{1,4}*

¹University of Arizona, Department of Chemistry & Biochemistry, 1306 E. University Blvd.,
Tucson, AZ 85721, USA

²Brookhaven National Laboratory, Center for Functional Nanomaterials
Upton, NY 11973, USA

³Department of Electrical & Computer Engineering, University of Nebraska-Lincoln, Lincoln,
NE 68588, USA

⁴University of Arizona, Department of Physics, 1118 E. Fourth Street, Tucson, AZ 85721, USA

KEYWORDS TiOPc, Cu(110), STM, UPS, 2PPE, molecular self-assembly

We use low-temperature scanning tunneling microscopy in combination with angle-resolved ultraviolet and two-photon photoemission spectroscopy to investigate the interfacial electronic structure of titanyl phthalocyanine (TiOPc) on Cu(110). We show that the presence of two unique molecular adsorption configurations is crucial for a molecular-level analysis of the hybridized interfacial electronic structure. Specifically, thermally induced self-assembly exposes marked adsorbate-configuration specific contributions to the interfacial electronic structure. The

results of this work demonstrate an avenue towards understanding and controlling interfacial electronic structure in chemisorbed films even for the case of complex film structure.

I. INTRODUCTION

Organic semiconductors have already found mainstream use in modern optoelectronic devices such as organic photovoltaics,¹ and stand poised to play a pivotal role in next-generation nanoelectronic devices.² Molecules are well suited for this role because their electronic eigenstates, and thus functional properties, can be readily tailored by structural modification via targeted synthesis. Molecular building blocks also promise new bottom-up avenues for device engineering at unprecedented length-scales.^{3,4} In devices, molecular materials serve e.g. as the active layers in transducing elements of photovoltaic cells and light-emitting diodes.⁵ Given the limited charge carrier mobility in molecular condensates,⁶ the active layer must at some point be coupled to a good electrical conductor. Interfacial energetics of these junctions must then be tailored to facilitate charge flow into and out of the device. A molecular-level understanding of interface formation is key to tailoring the electronic properties at such junctions. Hence, to harness the full potential of molecular materials in electronic devices, nanoscale studies of organic heterojunctions formed with metallic electrodes are of critical importance.

Great strides in our understanding of metal-organic heterojunctions have given rise to working models describing energy-level alignment regimes and interfacial electronic structure.⁷⁻¹⁰ Many of the proposed mechanisms underpinning energy-level alignment have been corroborated by both experiment and theory, at least in specific instances. In this context, the modification of the metal *surface dipole* is particularly relevant:^{11,12} This dipole, and therefore the work function, typically decrease as a result of molecular adsorption. This is due to a reduction in electron density “spill-out” from the metal surface, known as the push-back or pillow effect.¹³ The result

is a change in the electrostatic potential at the surface, i.e. the *interface dipole*, which also shifts the energies of the molecular levels. This simple picture describes the dominant interaction in *physisorbed* systems, and typically increases the hole-injection barrier if not counteracted by additional surface modifications.¹⁴ For *weakly chemisorbed* interfaces, higher order effects influencing energy-level alignment may be captured e.g. by the induced density of interface states model,¹⁵⁻¹⁷ or a general electrostatic density of states model.¹⁸ Despite these advances for weakly bound heterojunctions, the case of *strongly interacting and chemisorbed* interfacial electronic structure remains a challenge both experimentally and theoretically.

For this work, we define chemisorption as describing systems where the electronic wavefunction of the adsorbed molecule substantially hybridizes with that of the surface. This strong hybridization dramatically alters interface energetics and can lead to a wide range of phenomena including significantly broadened molecular levels, charge transfer, new interface states, new intermolecular interactions, and even metallic molecular monolayers.¹⁹⁻²³ One consequence of chemisorption is that such hybridized interfaces are frequently especially difficult to characterize. For example, renormalization and broadening of molecular levels complicates interpretation of electronic structure measurements made in the laboratory;²⁴ at the same time, correctly treating dispersive interactions, fractional charge-transfer, and disordered systems are formidable obstacles in computation and theory.^{25,26} Electronic structure measurements must be combined with real-space structural information on atomic length-scales, since a precise understanding of the microscopic interfacial structure is an essential ingredient if the principles at work in strongly coupled systems are to be understood.

To this end, scanning probe microscopies have become imperative for investigating molecular interfaces. The scanning tunneling microscope (STM) is especially well-suited for probing the

electronic effects of interface formation by combining sub-angstrom spatial resolution with electronic structure information in the form of image contrast and tunneling spectra (scanning tunneling spectroscopy, STS), which has been used to great effect in the case of a number of strongly interacting organic semiconductor interfaces.^{27,28} In conjunction with photoemission, the complementary techniques can provide even deeper and crucial insight into the forces driving the electronic structure of interfacial systems.²⁹

To further our understanding of strongly coupled and complex systems, we present here the study of a prototypical chemisorbed interface where unique interactions of two unique adsorbate configurations are used to disentangle the interfacial electronic structure in configuration-specific detail. We investigate room temperature grown thin-films of TiOPc on Cu(110) by low-temperature STM and angle-resolved photoemission spectroscopy. We then initiate self-assembly to alter the adsorption environment primarily for one adsorbate configuration. This allows us to elucidate changes in the interfacial density of states (DOS), and to identify differences in surface-molecule coupling for different molecular configurations. Our work demonstrates how such an approach is useful to develop a tractable framework for understanding and controlling chemisorbed interfacial electronic structure even for complex adsorbate systems.

II. METHODS

Cu(110) was cleaned by repeated cycles of Ar⁺ sputtering (1-2 keV, 5-10 $\mu\text{A}/\text{cm}^2$) and annealing (850 K). Cleanliness of the bare surface was verified directly in STM images or by the work function in ultraviolet photoemission spectroscopy (UPS). TiOPc (Sigma-Aldrich, 95%) was triply resublimated in a custom-built vacuum furnace (5×10^{-7} torr). Thin-films of TiOPc were evaporated onto room temperature Cu(110) using a home-built, water-cooled Knudsen source in a sample preparation chamber (base pressure $< 1 \times 10^{-9}$ torr). Film growth, at a typical

rate of 0.1 monolayer/min, was monitored by quartz crystal microbalance and calibrated with STM. Film thickness is reported as a fraction of a hypothetical closed monolayer (ML) and corresponds to the percentage of substrate surface area covered (1 ML \approx 4.44×10^{13} molecules/cm²).

In STM experiments, the sample was transferred to the imaging chamber (pressure $< 10^{-11}$ torr) immediately following surface preparation, and held at room temperature for 2 min before rapid quenching to 77 K and continued cooling to 5 K. All STM images shown were acquired at 5 K using an electrochemically etched tungsten tip in constant current mode. Microscope control and image processing were performed using the GXSM software package.³⁰ In photoemission experiments (analysis chamber pressure $< 10^{-10}$ torr), all spectra shown were collected at room temperature with the emission angle normal to the surface. Photon sources include an unpolarized

Scientific Instruments UVS 200 He lamp, and a Spectra-Physics Tsunami 80 MHz Ti:Sapphire laser, frequency-doubled to output 80 fs pulses centered at 373 nm. Analyzer resolution is approximately 70 meV as determined by Fermi level broadening of the clean Cu(110) surface. Sample temperature during film annealing was monitored proximally via a thermocouple attached to the button heater or directly on the crystal surface via infrared pyrometer for STM and photoemission experiments, respectively. Gas phase density functional theory (DFT) calculations were performed in Gaussian09 with the B3LYP hybrid functional and a 6-31G basis set.

III. RESULTS

The surface-normal UPS spectrum for clean Cu(110) is given in Figure 1a (black line). Two sets of sharp emission features between -2 and -5 eV binding energy (BE) mark direct transitions

from the d-band DOS with Σ symmetry.³¹⁻³⁴ The intensity ratio of the highest peaks in each set ($\sim 5:1$) along with a work function of $\phi = 4.5(1)$ eV demonstrate the surface cleanliness prior to molecular adsorption.³⁵ Two more features near E_F are satellite He I β emission from the intense Cu d-bands. Overlaid is the spectrum of 0.5 ML TiOPc grown on room temperature Cu(110) (blue line; see Figure 5c for a close-up of the frontier orbital region). Relative to bare Cu(110), the molecular interface shows a work function drop of ~ 0.3 eV, consistent with push-back. The ratio of the d-band features decreases and the widths of the peaks broaden due to scattering by the adsorbates. Already at this coverage, small contributions to the photoemission intensity from the molecular DOS develop below the Cu features in the regions labeled M1, M2, and M3. A very slight increase in intensity is also observed in the region near E_F (labeled FO, frontier orbitals) but is somewhat obscured by the He I β satellite emission peaks.

We include calculated gas phase density functional theory (DFT) molecular orbitals below the spectrum to provide an approximate broad indication of the predominant identity of the molecular DOS regions discussed throughout the text. Table 1 provides a summary of the typical orbital character in each region: Region M1 contains deeper lying molecular orbitals with mainly σ symmetry (electron density in the heterocycle plane), mostly without Ti character, and no density on the O atom. Region M2 is composed of the orbitals lying just below the Cu d-bands with again mainly σ symmetry and moderate Ti-O character. We associate region M3 with

Table 1. DFT Molecular Orbital Character

Region	Orbital Symmetry	Titanium Character	Oxygen Character
M1	σ	Low	None
M2	σ	Moderate	Low-Moderate
M3	π	High-Low Mix	High-Low Mix

molecular orbitals that have predominantly π symmetry (electron density out of the heterocycle plane), some with high and some with low Ti-O character. The simple gas phase calculations are intended to serve as a coarse guide to the spectrum. A full treatment of the molecular character in regions M1-3 would require proper inclusion of interfacial exchange-correlation effects and of the quasiparticle levels truly probed in the experiment, which is beyond the scope of the present work.

A constant current STM image of the 0.5 ML film is shown in Figure 1b. The STM image captures two unique molecular adsorption configurations and their predominant adsorption environments. Because TiOPc lacks inversion symmetry, two general adsorption configurations are realized, depending on the orientation of the titanyl moiety (Figure 2). As detailed in prior work, the species with a central feature of bright contrast is assigned to the configuration with the oxygen atom directed toward the surface (“O-down”).³⁶ This assignment is supported by asymmetry in the molecule, both in terms of interlobe distances and apparent lobe heights, which reflect a tilted molecular geometry on the surface. Conversely, the four-fold symmetric species with no central feature reflects a flat adsorption geometry on the surface and is assigned to the “O-up” configuration.³⁶ The two configurations have different dipole orientations and orbital overlap with the surface, and are thus subject to unique configuration-dependent interfacial interactions. For example, dispersive interactions with the ligand favor adsorption coplanar with the surface and at terrace sites for “O-up” adsorbates (Figure 1b). Meanwhile, electrostatic interactions between the charge distributions of the molecule and the step edge play a more prominent role in “O-down” adsorbates and lead to preferential adsorption at these sites.³⁶

Figure 3a gives the UPS spectrum for a 1 ML film as grown on the room temperature substrate (see Fig. 5c for a close-up of the frontier orbital region). The adsorption of additional molecules

enhances push-back to further decrease the work function to $\varphi_{1ML} \approx 4.1$ eV for a total change of $\Delta\varphi_{ads} \approx -400$ meV compared to bare Cu(110). As bare surface features give way to molecular features, clusters in the molecular DOS become readily distinguishable, separating near binding energies of -5.2 and -7.8 eV. At this coverage, two peaks are resolved in the frontier orbital region at approximately -1.5 eV and -0.15 eV binding energy, respectively (see Figure 5c below for a close-up of this spectral region). We assign these two features to the HOMO and the partially filled LUMO of TiOPc. This assignment is consistent with the observation of a partially filled former LUMO (*f*-LUMO) of TiOPc on Ag(100) and Ag(111). An *f*-LUMO is expected on Cu(110) as well since this surface is both more reactive and has a lower work function (~ 200 meV) relative to Ag(111). Each of these factors shifts the LUMO further below E_F , thus supporting our assignment.^{24,37–39} The accompanying STM image (Figure 3b) shows amorphous film growth for a surface coverage near 1 ML, which is corroborated in angle-resolved UPS by the fact that all molecular features are nondispersive.⁴⁰ Interspersed in the amorphous film are small aggregates of primarily “O-down” molecules (regions of bright contrast on the terrace) which are decorating small islands of Cu adatoms.³⁶

The heterogeneous nature of the as-grown film seemingly complicates a detailed interpretation of interfacial energetics, because each molecular configuration contributes to the measured DOS in potentially non-trivial ways. We show here however that the existence of two adsorption configurations provides instead a handle for tuning the physical and electronic structure of the system, from which a deeper understanding of interfacial energetics is obtained. A dramatic thermally-driven surface coarsening was demonstrated for several members of the Pc family on Cu(110),⁴¹ and we showed previously that for TiOPc, this involves a configuration-selective process of cooperative self-assembly between Cu adatoms and “O-down” molecules (Figure 4).³⁶

Insight from this configuration-specific process is key to understanding the electronic structure transformation that accompanies surface texturing.

Figure 5a gives comparison photoemission spectra for 1 ML TiOPc thin-films before and after self-assembly. The work function change, relative to bare Cu(110), for the surface textured by self-assembly is $\Delta\varphi_{SA} \approx -260$ meV, indicating that the work function rises by ~ 140 meV from the as-deposited film. Furthermore, self-assembly causes a significant decrease in photoemission intensity in regions M1 and M2. A decrease is observed also in region M3, however the spectral profile remains largely intact. Figures 5b and 5c are photoemission spectra taken with a restricted analyzer acceptance angle ($\pm 1.5^\circ$) to improve resolution and to remove Cu contributions away from $\bar{\Gamma}$. The spectrum in Figure 5b makes the intensity changes in region M1 and especially M2 particularly clear, and shows that the dip in intensity between the two regions is significantly weaker.

Changes to the frontier orbitals are also visible in the UPS data. Figure 5c shows an intensity decrease in both the HOMO and f -LUMO following self-assembly. We studied this region in more detail by supplementing UPS with 2PPE to take advantage of larger apparent cross-sections for hybrid interface states in 2PPE.^{42,43} Furthermore, the linearly-polarized excitation source in 2PPE reduces background contributions by decreasing the number of symmetry allowed transitions for photoemission from the Cu surface.³¹ While scanning tunneling spectroscopy (STS) is well established for locally probing frontier orbitals and interface states in adsorbate systems, we showed previously that molecular features in STS of TiOPc on Cu(110) are obscured by broadening from hybridization with the surface.⁴⁴ Thus we concentrate on the photoemission results to understand the chemisorptive environment in more detail. Figure 6 shows 2PPE spectra for a 0.87 ML film before and after thermal annealing (\vec{E} in the ΓKLU

plane and p-polarized to sample surface). We use a photon energy of 3.3 eV to probe just deep enough into the occupied manifold to investigate the frontier orbital features, while avoiding one-photon induced photoemission. At this photon energy, the number and energies of the observed features are consistent with UPS, demonstrating that no intermediate states were probed. Since we are therefore only considering occupied states, we are thus able to continue to use the binding energy scale also used in UPS.⁴⁵ The enhancement in hybrid interface states relative to the unstructured photoemission background from Cu(110) is indeed marked in 2PPE and, importantly, facilitates a quantitative analysis of the observed changes (Figure 6).

From STM it is known that the two molecular configurations couple differently to the surface and have unique dipole orientations.^{36,44} Each configuration is therefore expected to present a different electronic structure. The *f*-LUMO region thus consists at least of two contributions, each associated with one specific molecular configuration, and clearly visible in the strongly asymmetric spectroscopic *f*-LUMO feature. This yields a minimal model where we neglect a potential lifting of the LUMO degeneracy,⁴⁴ which would lead to further fine structure in the *f*-LUMO region that is not resolved in the data (Figure 6).⁴⁶ We thus fit the *f*-LUMO region using two Gaussian functions, each modified by a Fermi-Dirac distribution $f(E)$, to capture the *f*-LUMO for each adsorption configuration located near E_F :

$$I(E) = A_0 e^{\frac{(E-E_0)^2}{A_1}} \cdot f(E) \quad (1)$$

The spectral background is derived from a bare Cu(110) spectrum and can be treated as a nearly constant contribution e.g. from the non- k conserving Cu s,p-band transitions below E_F .³⁵ Multiplication by the Fermi-Dirac distribution adequately captures the spectral envelope of partially occupied molecular states, as observed also at other metal/organic interfaces.^{22,24,47} Both the background and $f(E)$ parameters were determined on bare Cu(110) and constrained

permanently, leaving six adjustable parameters to fit the data (amplitude, width, and center for each Gaussian). Our configuration assignments of each feature are described in the next section.

In this minimal model, the f -LUMO contributions from both configurations are strongly overlapping and extend potentially beyond E_F . The latter point is supported by the fact that the spectral shape at E_F is effectively captured by equation (1). An unconstrained fit with two Gaussians establishes the important fact that both features shift toward lower binding energy upon SA. The unconstrained fit is however unsatisfactory for two reasons: *i*) Strong correlation between parameters, and *ii*) unphysical peak amplitudes and widths, corresponding to drastically different number densities for the two molecular configurations on the surface. This is at variance with the STM results (Figure 4, and discussed in more detail below) which demonstrate clearly that “O-up” and “O-down” are present in close to a 1:1 ratio, and might instead imply that photoemission yields differ by more than a factor of 5 between the two configurations. This is however unlikely, because the STM data show that prior to SA “O-down” molecules adsorbed on terraces are tilted only by a rather small amount. Selection rules and photoemission cross-section are thus expected to be similar for both configurations prior to SA.⁴⁸

These findings enable us to constrain the spectral decomposition in a global fitting routine involving both the spectra before and after SA to enable a robust analysis of the f -LUMO feature. Since neither adsorption geometry nor surface-density of “O-up” molecules change during SA, we fix all parameters except the peak center for this configuration. Furthermore, for the as-grown film we constrain the integrated intensity from the full Gaussian band profile for both “O-up” and “O-down” features to be comparable (within a factor of 1.65), reflecting their similar photoemission cross-section and orientation relative to the surface normal.

This procedure reveals that before annealing, the lower binding energy f -LUMO peak (colored light blue in Figure 6b and assigned to “O-up” TiOPc as discussed below) is centered at a binding energy $E_b = -90(10)$ meV, i.e. below E_F , with a full width at half maximum (FWHM) of 595(22) meV. The higher binding energy f -LUMO (colored green in Figure 6b and assigned to “O-down” TiOPc) is centered at $E_b = -149(4)$ meV with a FWHM of 337(8) meV. Following the annealing step, the “O-up” f -LUMO shifts to $E_b = -34(5)$ meV (FWHM 595(22) meV), and the “O-down” f -LUMO shifts to $E_b = +60(20)$ meV (above E_F) with FWHM = 380(32) meV. We emphasize that under the chosen assumptions these results are robust and only minimally correlated. The strong similarity between the photoemission spectra in Figures 5c and 6a (different photon energies and coverages) also demonstrate that our findings are robust with respect to film coverage within the range that cooperative self-assembly is observed. We discuss the implications of these findings in the next section.

IV. DISCUSSION

To better understand the forces that shape the interfacial electronic structure, we apply insight from the nanoscale imaging to help interpret the photoemission data. We begin by summarizing the key observations from both experimental approaches, each of which confirms a strong chemisorption regime for this system: *i*) In STM, we observe just a few molecular registries with the Cu(110) lattice for each configuration, one registry for “O-up” and two equivalent registries for “O-down”, indicating a small set of dominant interactions with the surface, likely between a small group of atoms in the molecule and on the surface (Figures 1b and 3b).³⁶ *ii*) In photoemission, molecular orbital energies do not simply track the change in work function (Figures 1a, 3a, and 6). Together these observations point to significant surface-molecule coupling and a strongly hybridized interfacial electronic structure. We show that despite the

strong hybridization the electronic structure can be parsed because of the existence of the two distinct molecular adsorption configurations.

Before we discuss specific spectral features, we start with collective contributions to the surface work function at higher surface coverages. The molecular-level structural detail of the TiOPc/Cu(110) interface shown in Figure 3b reveals that the global work function, measured by the secondary cutoff in UPS, stems in part from a complex mixture of electrostatic contributions.⁴⁹ From the STM data we know that step edges are fully saturated, predominantly by “O-down” TiOPc molecules, with appreciable populations of both molecular configurations and individual Cu adatoms distributed across the terraces (Figures 3b and 4a). Each molecular configuration possesses an intrinsic dipole moment, contributes a certain degree of push-back, hybridizes with the surface to a different extent, and induces image charges within the metal.⁹ Furthermore, electron density smoothing near Cu adatoms and step edges also alters the local charge distribution, and all of these local environments contribute to the electrostatic potential at the surface, $V(x, y, z)$.⁵⁰ The cartoon in Figure 7a portrays a sample of adsorbate and defect components that contribute locally to the electrostatic potential, indicated at some specific height z above the surface.^{9,51} Taken together, these local factors determine the globally averaged barrier to electron escape from the surface, i.e. the work function measured in UPS. The net result of molecular adsorption is a decrease of the work function through a balance of pushback and step-edge saturation.

The established interface dipole and HOMO-LUMO gap renormalization results in LUMO DOS tailing below E_F (Figure 6a and 8b), and enables partial electron transfer to the molecule (Figures 5c and 6b). Again, a partially filled f -LUMO for TiOPc on Cu(110) is expected given reports of a f -LUMO for TiOPc and CuPc on Ag(111),³⁷ and other phthalocyanines on

Cu(110).⁵² Charge flow out of the surface and into the molecule counteracts push-back effects, and equilibrium is reached at $\Delta\varphi_{ads} = -400$ meV for 1 ML coverage. The resulting *f*-LUMO feature of the as-deposited film is centered just below E_F (Figures 6 and 8). We note that with the HOMO located at $E_b \approx 1.5$ eV, the HOMO-LUMO gap has renormalized to ~ 1.4 eV.

Upon annealing, cooperative self-assembly gives rise to arrays of elongated Cu islands decorated almost entirely with adsorbed “O-down” TiOPc (Figure 4). The ~ 140 meV increase ($\Delta\Delta\varphi$, Figure 8c) of the global work function ensuing self-assembly ($\Delta\varphi_{SA}$) cannot be explained by patterning of the surface with Cu islands: An increase in steps edges should decrease the work function, contrary to our observation. Instead, $\Delta\varphi_{SA}$ likely results primarily from the reorientation of free “O-down” TiOPc dipoles once adsorbed at step edges as part of the nanoribbon. Changes in apparent height and image contrast of “O-down” molecules show that these dipoles are directed further from surface normal after self-assembly (Figures 4 and 7). Both the considerable dipole moment for TiOPc (3.7 D calculated in the gas phase), which persists in large measure following adsorption,⁵³ and the efficiency of self-assembly in reorienting nearly all “O-down” molecules (Figure 4b) support molecular orientation as a key factor in the observed work function increase.

Self-assembly predominantly alters the local electronic environments of “O-down” TiOPc molecules, which have moved from terrace sites to the step edges of Cu adatom islands (Figure 7b). The fits in Figure 6 capture the local electronic environment by resolving the *f*-LUMO feature into two peaks, one for each molecular configuration. The binding energy of each peak indicates transfer of at least one full electron into the *f*-LUMO for both configurations. This is corroborated by a recent study of the Kondo effect in this system that proves the existence of an

unpaired spin in TiOPc adsorbates on Cu(110).⁴⁴ Since STM shows that the molecular structure remains intact regardless of adsorption site, we may assign the two f -LUMO peaks to the individual configurations in the as-grown film as follows: The smaller binding energy and broader f -LUMO is assigned to the “O-up” configuration due to stronger coupling of the “O-up” TiOPc π -system to the surface. This increases screening of the photohole and broadens the DOS, despite a dipole orientation that would otherwise favor a shift to larger binding energies.⁵⁴ The frontier orbitals are dominated by the conjugated π -system of the heterocycle, and the overlap with the surface electronic wavefunction is thus more extensive in “O-up” adsorbates.³⁸ The narrower, higher binding energy f -LUMO is assigned to “O-down” TiOPc, consistent with this interpretation: Less surface wavefunction overlap reduces broadening of the f -LUMO DOS and decreases photohole screening in “O-down” adsorbates, resulting in a larger ionization energy. We will show below that this interpretation is supported by all our findings.

Upon self-assembly, the combined f -LUMO DOS shifts to lower binding energy, following the direction of $\Delta\phi_{SA}$; remarkably though, the individual f -LUMO components do not track the global work function change quantitatively. Together with an apparent change in the combined peak shape, this is indicative of two distinct molecular populations whose ionization energies respond differently to the film transformation during self-assembly. The “O-down” f -LUMO peak shifts by $\sim+205$ meV into the unoccupied manifold above E_F , while the “O-up” f -LUMO shifts toward E_F by only $\sim+50$ meV (Figure 8c). The observed energy shifts clearly indicate that self-assembly alters the electronic structure of each molecular configuration to very different degrees. The local environment of “O-up” TiOPc is affected only by the proximity of nanoribbons (Figures 4 and 7), changing the “O-up” electronic structure only minimally, as borne out by the robust fit. In contrast, the larger energy shift for the “O-down” f -LUMO reflects

the new local electronic environment for molecules in the nanoribbons (Figure 7b): Interface dipole effects and altered surface-molecule coupling decrease the f -LUMO ionization energy and broaden the f -LUMO DOS. In summary, different local electronic environments account for the observed changes in f -LUMO binding energies for both configurations before and after self-assembly.

The spectra in Figures 5 and 6 shows that the HOMO (1.5 eV binding energy) exhibits similar changes during self-assembly by shifting toward E_F and losing intensity. Due to a low spectral density and the substantial tail of the Cu d-band, the HOMO feature becomes nearly indistinguishable from the background in Figure 5a, precluding a configuration specific analysis. The qualitative observation of how self-assembly alters the collective HOMO hybridization with the surface is, however, in agreement with the findings for the f -LUMO region. In all, our central finding is that the two adsorption configurations lead to unique surface-molecule coupling regimes that give controllable energy level alignment in the frontier orbitals by thermally induced self-assembly.

Interpreting the chemisorbed electronic structure in detail is not limited to the frontier orbitals. Figure 5b shows that deeper levels also evolve to reflect the change in electrostatic potential and interfacial electronic interactions that accompany self-assembly, with an especially pronounced modification to the DOS in regions M1 and M2. As demonstrated above, self-assembly drastically alters the adsorption environment and surface-coupling primarily for “O-down” TiOPc, and we can therefore attribute changes in regions M1 and M2 specifically and primarily to this adsorption configuration. Moving to a step edge upon nanoribbon formation redistributes the photoemission intensity in these energy regions by changing the interaction with the surface, distorting the molecule, or altering the photoemission cross-section. For these same reasons,

transitions leading to the features in region M3 are dominated by “O-up” TiOPc, since these molecules remain essentially unaltered following self-assembly. This is again supported by the gas phase electronic structure calculations: If originating from “O-down” molecules, the Ti and O character of many orbitals in M3 would render these features extremely sensitive to the changing adsorption environments, which is not observed. Changing interfacial electronic structure well below the frontier orbitals introduces one final point: Hybridization with the surface occurs not only near E_F , but also for lower energy states. These lower lying orbitals are often overlooked, but may provide a pathway for charge back-donation to offset the extent of charge transfer accompanying f -LUMO formation.^{55,56}

V. CONCLUSIONS

While configuration-specific aspects of photoemission have been inferred in studies of weakly interacting surfaces,⁵⁷ this work demonstrates a remarkable instance where the *chemisorbed* interfacial electronic structure can be uncovered at a fundamental level on the basis of two simultaneous yet chemically different adsorbate configurations. In analyzing the TiOPc/Cu(110) interface, we have shown that these two distinct molecular adsorption configurations contribute independently to the interfacial electronic structure. Dissecting these contributions is achieved by considering the local adsorption environments, coupling regimes, and interactions of individual molecules while thermally restructuring the surface. Furthermore, our emphasis on characterizing the nature of the surface-molecule interactions highlights an important mode of control over interfacial energetics, i.e. finding structural motifs that can drive energy-level alignment in strongly chemisorbed systems.

To summarize our overall findings, we show that a strongly interacting interface with complex film structure can be readily understood through the presence of two discrete molecular

adsorption configurations. Interfacial interactions unique to each configuration offer control over configuration-selective surface processes that tune the electronic structure in molecular subsets, and their contrast illuminates the origin and importance of various competing interactions. We have thus developed an improved understanding of the interfacial electronic structure at a complex chemisorption interface over an extended energy scale. This comprehensive interpretation of chemisorbed interfacial electronic structure provides new ground on which to compare the results of theory with experiment to ultimately improve our understanding of such strongly interacting systems.

ACKNOWLEDGMENTS

This research was supported by the National Science Foundation under grants # CHE-1213243 and CHE-1565497 as well as the Arizona TRIF imaging fellowship. This research also used resources of the Center for Functional Nanomaterials, which is a U.S. DOE Office of Science Facility, at Brookhaven National Laboratory under Contract No. DE-SC0012704. P.S. acknowledges support by the U.S. Department of Energy, Office of Basic Energy Sciences under grant No. DE-SC0016343.

*monti@u.arizona.edu

¹ K.A. Mazzio and C.K. Luscombe, *Chem. Soc. Rev.* **44**, 78 (2015).

² L. Zang, Y. Che, and J.S. Moore, *Acc. Chem. Res.* **41**, 1596 (2008).

³ J. Björk and F. Hanke, *Chem. – A Eur. J.* **20**, 928 (2014).

⁴ J. V. Barth, *Annu. Rev. Phys. Chem.* **58**, 375 (2007).

⁵ P.M. Beaujuge and J.M.J. Fréchet, *J. Am. Chem. Soc.* **133**, 20009 (2011).

⁶ C.D. Dimitrakopoulos and P.R.L. Malenfant, *Adv. Mater.* **14**, 99 (2002).

- ⁷ H. Ishii, K. Sugiyama, E. Ito, and K. Seki, *Adv. Mater.* **11**, 605 (1999).
- ⁸ S. Braun, W.R. Salaneck, and M. Fahlman, *Adv. Mater.* **21**, 1450 (2009).
- ⁹ O.L.A. Monti, *J. Phys. Chem. Lett.* **3**, 2342 (2012).
- ¹⁰ J.B. Neaton, M.S. Hybertsen, and S.G. Louie, *Phys. Rev. Lett.* **97**, 216405 (2006).
- ¹¹ N.D. Lang and W. Kohn, *Phys. Rev. B* **3**, 1215 (1971).
- ¹² D. Cahen and A. Kahn, *Adv. Mater.* **15**, 271 (2003).
- ¹³ N. Koch, A. Kahn, J. Ghijsen, J.J. Pireaux, J. Schwartz, R.L. Johnson, and A. Elschner, *Appl. Phys. Lett.* **82**, 70 (2003).
- ¹⁴ G. Heimel, L. Romaner, E. Zojer, and J.-L. Bredas, *Acc. Chem. Res.* **41**, 721 (2008).
- ¹⁵ H. Vázquez, W. Gao, F. Flores, and A. Kahn, *Phys. Rev. B* **71**, 041306 (2005).
- ¹⁶ H. Vázquez, F. Flores, R. Oszwaldowski, J. Ortega, R. Pérez, and A. Kahn, *Appl. Surf. Sci.* **234**, 107 (2004).
- ¹⁷ C.S. Lee, J.X. Tang, Y.C. Zhou, and S.T. Lee, *Appl. Phys. Lett.* **94**, 1 (2009).
- ¹⁸ M. Oehzelt, N. Koch, and G. Heimel, *Nat. Commun.* **5**, 4174 (2014).
- ¹⁹ T.-C. Tseng, C. Urban, Y. Wang, R. Otero, S.L. Tait, M. Alcamí, D. Écija, M. Trelka, J.M. Gallego, N. Lin, M. Konuma, U. Starke, A. Nefedov, A. Langner, C. Wöll, M.Á. Herranz, F. Martín, N. Martín, K. Kern, and R. Miranda, *Nat. Chem.* **2**, 374 (2010).
- ²⁰ B.W. Caplins, D.E. Suich, A.J. Shearer, and C.B. Harris, *J. Phys. Chem. Lett.* **5**, 1679 (2014).
- ²¹ J. Zirotto, F. Forster, A. Schöll, P. Puschnig, and F. Reinert, *Phys. Rev. Lett.* **104**, 233004 (2010).
- ²² G. Heimel, S. Duhm, I. Salzmann, A. Gerlach, A. Strozecka, J. Niederhausen, C. Bürker, T. Hosokai, I. Fernandez-Torrente, G. Schulze, S. Winkler, A. Wilke, R. Schlesinger, J. Frisch, B.

Bröker, A. Vollmer, B. Detlefs, J. Pflaum, S. Kera, K.J. Franke, N. Ueno, J.I. Pascual, F. Schreiber, and N. Koch, *Nat. Chem.* **5**, 187 (2013).

²³ M.C.E. Galbraith, M. Marks, R. Tonner, and U. Höfer, *J. Phys. Chem. Lett.* **5**, 50 (2014).

²⁴ Y. Zou, L. Kilian, A. Schöll, T. Schmidt, R. Fink, and E. Umbach, *Surf. Sci.* **600**, 1240 (2006).

²⁵ S. Ehrlich, J. Moellmann, and S. Grimme, *Acc. Chem. Res.* **46**, 916 (2013).

²⁶ A.J. Cohen, P. Mori-Sánchez, and W. Yang, *Science* **321**, 792 (2008).

²⁷ R. Temirov, S. Soubatch, A. Luican, and F.S. Tautz, *Nature* **444**, 350 (2006).

²⁸ A. Kraft, R. Temirov, S.K.M. Henze, S. Soubatch, M. Rohlfing, and F.S. Tautz, *Phys. Rev. B* **74**, 041402 (2006).

²⁹ N. Nicoara, E. Román, J.M. Gómez-Rodríguez, J.A. Martín-Gago, and J. Méndez, *Org. Electron. Physics, Mater. Appl.* **7**, 287 (2006).

³⁰ P. Zahl, T. Wagner, R. Möller, and A. Klust, *J. Vac. Sci. Technol. B* **28**, C4E39 (2010).

³¹ J. Hermanson, *Solid State Commun.* **22**, 9 (1976).

³² A. Goldmann, D. Westphal, and R. Courths, *Phys. Rev. B* **25**, 2000 (1982).

³³ E. Dietz and F.J. Himpsel, *Solid State Commun.* **30**, 235 (1979).

³⁴ H. Przybylski, A. Baalman, G. Borstel, and M. Neumann, *Phys. Rev. B* **27**, 6669 (1983).

³⁵ R. Courths and S. Hufner, *Phys. Rep.* **112**, 53 (1984).

³⁶ B. Maughan, P. Zahl, P. Sutter, and O.L.A. Monti, *J. Phys. Chem. C* **119**, 27416 (2015).

³⁷ I. Kröger, B. Stadtmüller, and C. Kumpf, *New J. Phys.* **18**, 113022 (2016).

³⁸ S. Colonna, G. Mattioli, P. Alippi, A. Amore Bonapasta, A. Cricenti, F. Filippone, P. Gori, A. Maria Paoletti, G. Pennesi, F. Ronci, and G. Zanotti, *J. Phys. Chem. C* **118**, 5255 (2014).

- ³⁹ L. Fernández, S. Thussing, A. Mänz, G. Witte, A.X. Brion-Rios, P. Cabrera-Sanfelix, D. Sanchez-Portal, and P. Jakob, *J. Phys. Chem. C* **121**, 1608 (2016).
- ⁴⁰ M. Wießner, J. Ziroff, F. Forster, M. Arita, K. Shimada, P. Puschnig, A. Schöll, and F. Reinert, *Nat. Commun.* **4**, 1514 (2013).
- ⁴¹ M. Abadía, R. González-Moreno, A. Sarasola, G. Otero-Irurueta, A. Verdini, L. Floreano, A. Garcia-Lekue, and C. Rogero, *J. Phys. Chem. C* **118**, 29704 (2014).
- ⁴² L.L. Kelly, D.A. Racke, P. Schulz, H. Li, P. Winget, H. Kim, P. Ndione, A.K. Sigdel, J.-L. Brédas, J.J. Berry, S. Graham, and O.L.A. Monti, *J. Phys. Condens. Matter* **28**, 94007 (2016).
- ⁴³ N. Ilyas and O.L.A. Monti, *Phys. Rev. B* **90**, 125435 (2014).
- ⁴⁴ B. Maughan, P. Zahl, P. Sutter, and O.L.A. Monti, *J. Phys. Chem. Lett.* 1837 (2017).
- ⁴⁵ M.P. Steele, L.L. Kelly, N. Ilyas, and O.L.A. Monti, *J. Chem. Phys.* **135**, 124702 (2011).
- ⁴⁶ K. Schönauer, S. Weiss, V. Feyer, D. Lüftner, B. Stadtmüller, D. Schwarz, T. Sueyoshi, C. Kumpf, P. Puschnig, M.G. Ramsey, F.S. Tautz, and S. Soubatch, *Phys. Rev. B* **94**, 205144 (2016).
- ⁴⁷ V. Feyer, M. Graus, P. Nigge, M. Wießner, R.G. Acres, C. Wiemann, C.M. Schneider, A. Schöll, and F. Reinert, *Surf. Sci.* **621**, 64 (2014).
- ⁴⁸ W.D. Grobman, *Phys. Rev. B* **17**, 4573 (1978).
- ⁴⁹ E. Goiri, P. Borghetti, A. El-Sayed, J.E. Ortega, and D.G. De Oteyza, *Adv. Mater.* **28**, 1340 (2016).
- ⁵⁰ R. Smoluchowski, *Phys. Rev.* **60**, 661 (1941).
- ⁵¹ O.L.A. Monti and M.P. Steele, *Phys. Chem. Chem. Phys.* **12**, 12390 (2010).
- ⁵² F. Hu, H. Mao, H. Zhang, K. Wu, Y. Cai, and P. He, *J. Chem. Phys.* **140**, 94704 (2014).
- ⁵³ H. Fukagawa, S. Hosoumi, H. Yamane, S. Kera, and N. Ueno, *Phys. Rev. B* **83**, 085304

(2011).

⁵⁴ S. Duhm, G. Heimel, I. Salzmann, H. Glowatzki, R.L. Johnson, A. Vollmer, J.P. Rabe, and N. Koch, *Nat. Mater.* **7**, 326 (2008).

⁵⁵ M. Gruenewald, L.K. Schirra, P. Winget, M. Kozlik, P.F. Ndione, A.K. Sigdel, J.J. Berry, R. Forker, J.-L. Brédas, T. Fritz, and O.L.A. Monti, *J. Phys. Chem. C* **119**, 4865 (2015).

⁵⁶ M. Toader, P. Shukrynau, M. Knupfer, D.R.T. Zahn, and M. Hietschold, *Langmuir* **28**, 13325 (2012).

⁵⁷ H. Yamane, H. Honda, H. Fukagawa, M. Ohyama, Y. Hinuma, S. Kera, K.K. Okudaira, and N. Ueno, *J. Electron Spectros. Relat. Phenomena* **137–140**, 223 (2004).

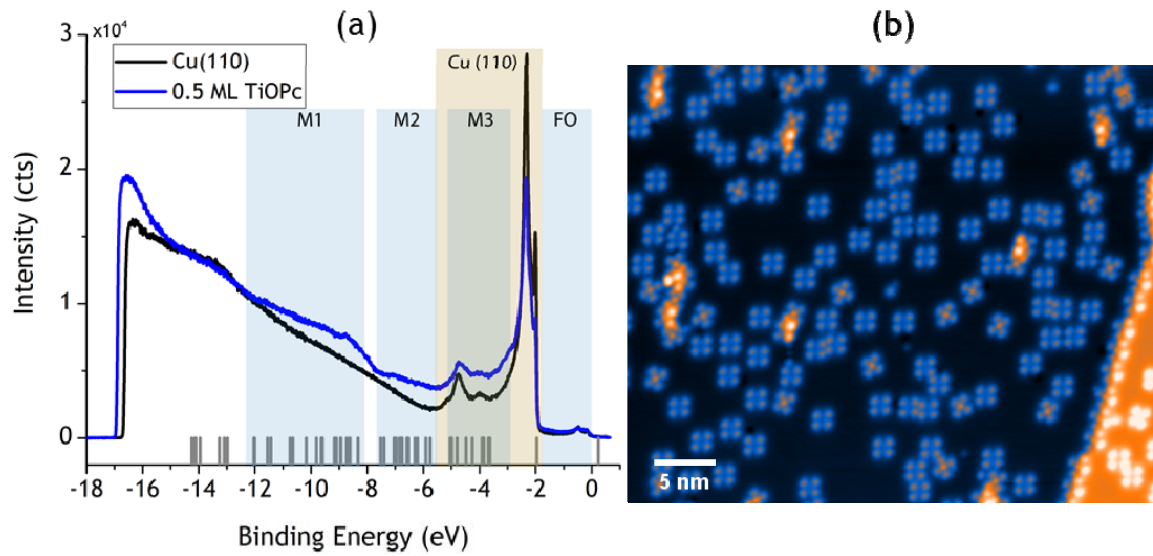


FIG. 1. (a) Surface-normal UPS spectra for clean Cu(110) (black) and 0.5 ML TiOPc (blue). Blue windows indicate spectral regions with molecular DOS, and the brown window indicates the spectral region for emission from Cu d-bands. The energy scale is referenced to the Fermi level (binding energy $E-E_F$). See Fig. 5c for a close-up of the frontier orbital region. (b) STM image of 0.5 ML TiOPc on Cu(110) (Sample bias $V_S = 5$ mV; tunneling current $I_T = 0.20$ nA).

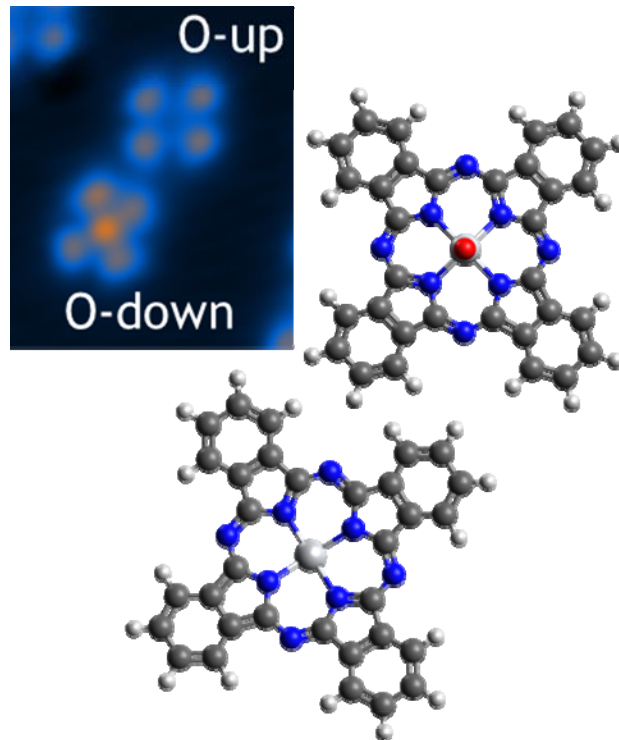


FIG. 2. TiOPc adsorption configurations. Molecules with the oxygen atom directed toward the surface are labeled “O-down” while those with the oxygen atom directed away from the surface are labeled “O-up”. STM image taken from Figure 1.

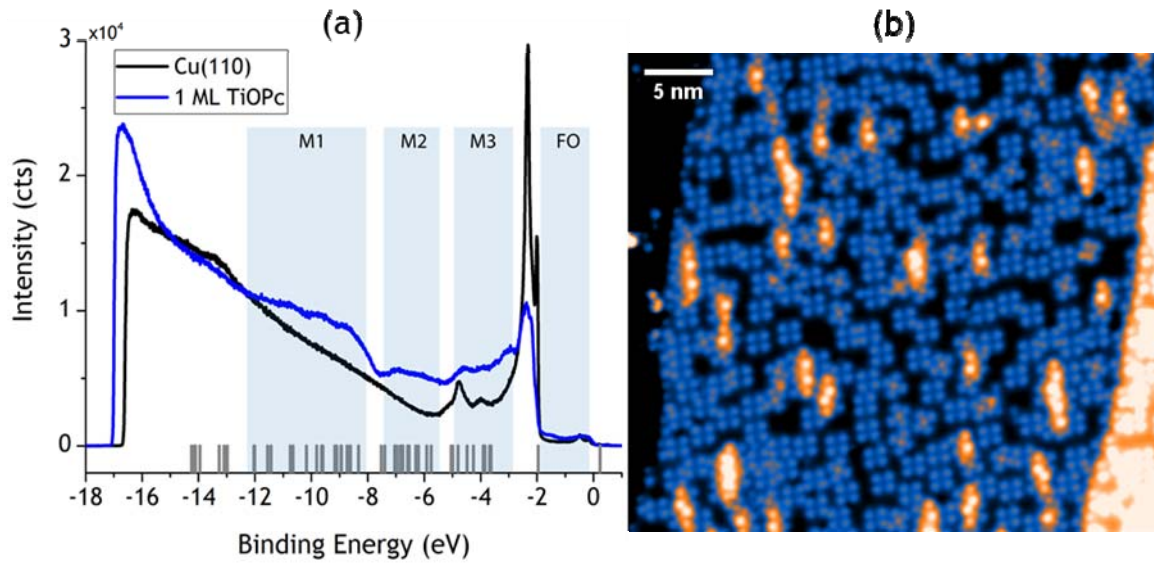


FIG. 3. (a) Surface-normal UPS spectra for clean Cu(110) (black) and 1 ML TiOPc (blue). See Fig. 5c for a close-up of the frontier orbital region. (b) STM image of near 1 ML TiOPc on Cu(110) ($V_s = 10$ mV, $I_T = 0.10$ nA).

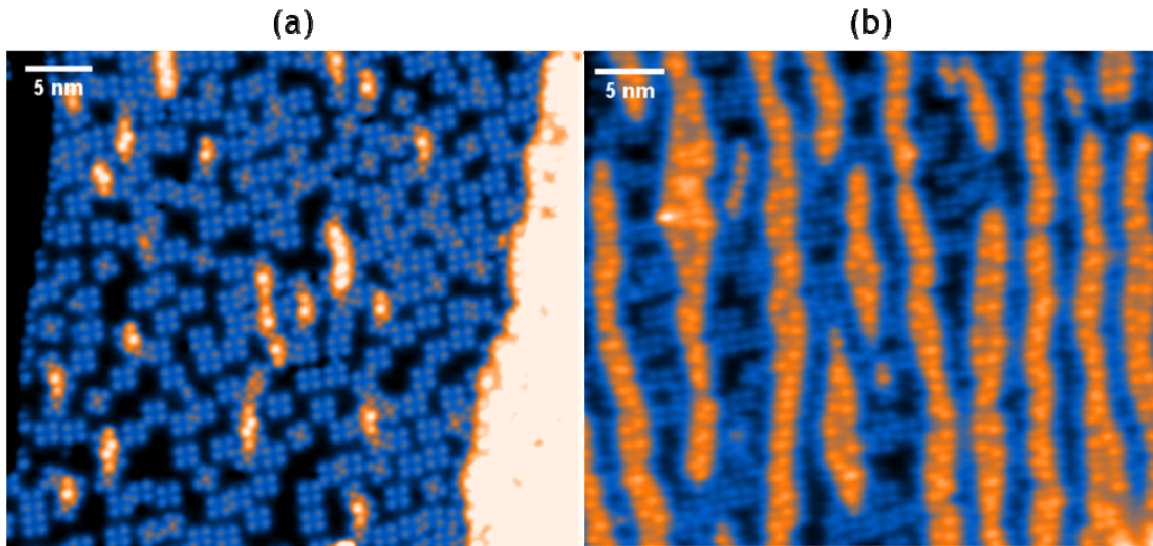


FIG. 4. (a) Room temperature grown film of near 1 ML TiOPc ($V_S = 50$ mV, $I_T = 0.10$ nA). (b) The same film after UHV annealing to 190 °C ($V_S = 10$ mV, $I_T = 0.10$ nA). The surface is coarsened by cooperative self-assembly of TiOPc with Cu adatoms.

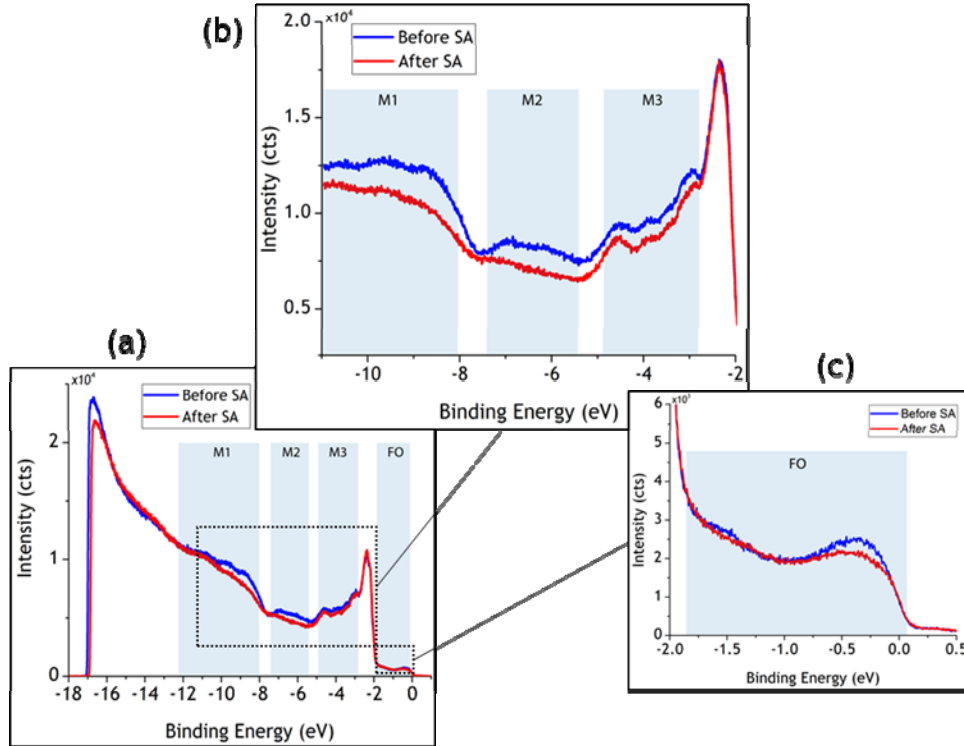


FIG. 5. (a) Survey ultraviolet photoemission spectra for 1 ML TiOPc on Cu(110) before (blue) and after (red) self-assembly ($V_S = -5$ V). (b) High resolution spectra for the M1, M2, and M3 molecular regions. Features in M1 and M2 change significantly upon self-assembly, while those in region M3 largely retain their original profile. (c) High resolution spectra for the frontier orbital region near E_F . In (b) and (c), the spectra were taken with a restricted analyzer acceptance angle of $\pm 1.5^\circ$ and $V_S = -3$ V.

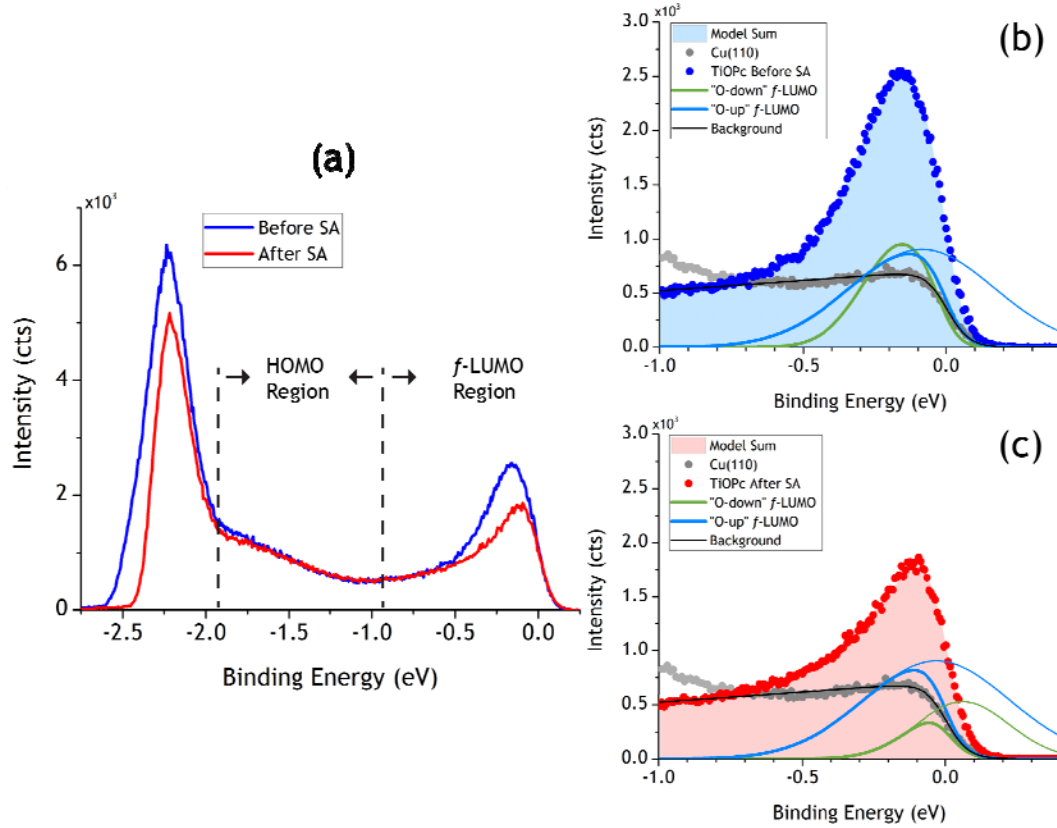


FIG. 6. (a) 2PPE spectra for 0.87 ML TiOPc on Cu(110) before (blue) and after (red) thermal annealing and self-assembly. Analyzer acceptance angle = $\pm 1.5^\circ$ and $V_S = -1.2$ V. (b) Fit of the *f*-LUMO region before self-assembly with two Gaussians modified by Fermi-Dirac functions (thick lines). The full Gaussian DOS extending into the unoccupied region is also shown (thin lines). The background is derived from clean Cu(110) data (grey) and the model sum is shown by the shaded area. (c) Fit of the *f*-LUMO region after self-assembly, as in (b).

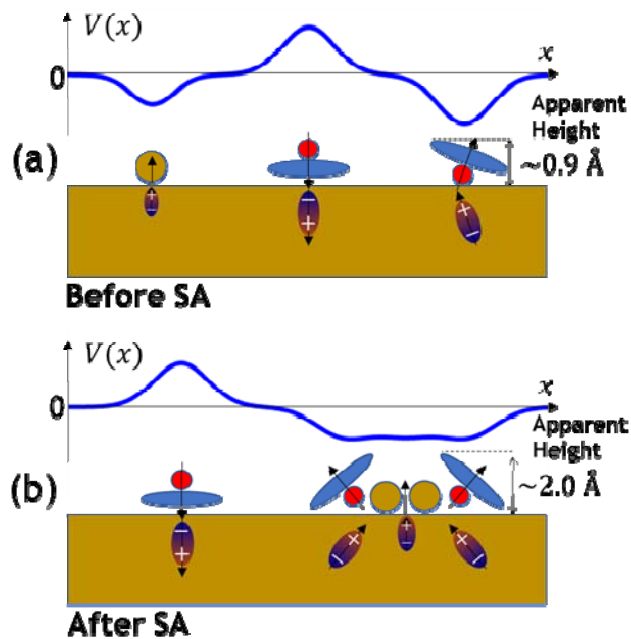


FIG. 7. Cartoon of local contributions to the electrostatic potential above the surface, $V(x, y, z)$, in a simplified point dipole picture. A cut through $V(x, y, z)$ at constant coordinate y and constant height z is shown above each cartoon, and associated image dipoles are shown beneath the surface. (a) Before self-assembly, free “O-down” molecules show an apparent height of $\sim 0.9 \text{ \AA}$ in STM images. (b) In self-assembly, adatoms coordinate with “O-down” molecules to form nanoribbons and reorient the “O-down” dipole moment. “O-down” molecules in these nanoribbons show an apparent height of $\sim 2.0 \text{ \AA}$.

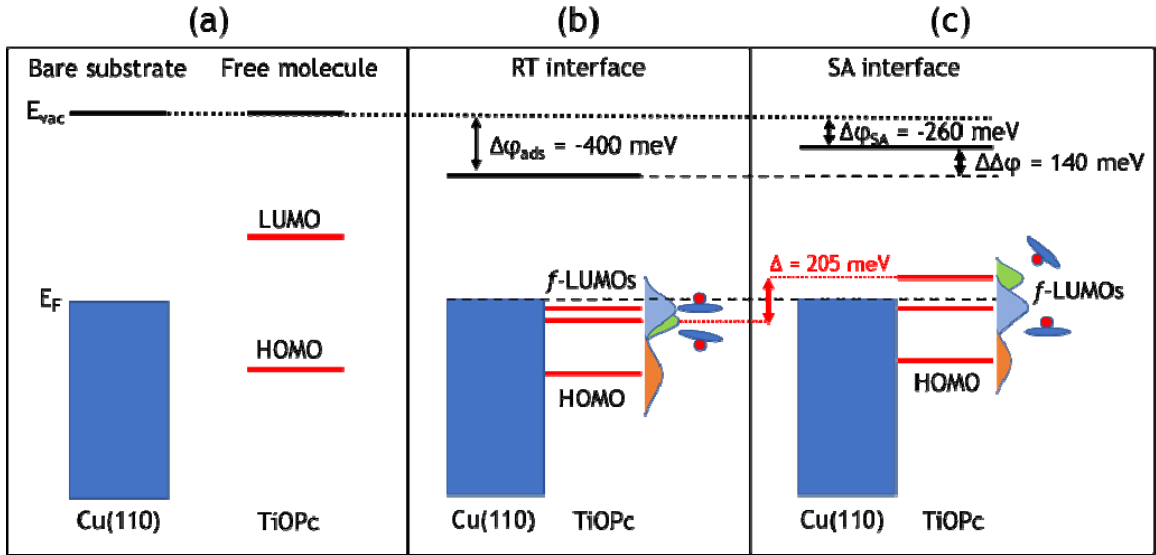


FIG. 8. (a) Energy level diagram for Cu(110) and free TiOPc. (b) Upon adsorption, the work function change and energy renormalization bring the LUMO DOS below E_F (f -LUMO). (c) After configuration-selective self-assembly, the f -LUMO DOS for “O-down” TiOPc shifts above E_F while the f -LUMO DOS for “O-up” changes only slightly.